AIAA JOURNAL
Vol. 31, No. 8, August 1993

Analysis of Passive Damping in Thick Composite Structures

D. A. Saravanos*
Ohio Aerospace Institute, Brookpark, Ohio 44142

Computational mechanics for the prediction of damping and other dynamic characteristics in composite structures of general thicknesses and laminations are presented. Discrete layer damping mechanics that account for the representation of interlaminar shear effects in the material are summarized. Finite element based structural mechanics for the analysis of damping are described, and a specialty finite element is developed. Applications illustrate the quality of the discrete layer damping mechanics in predicting the damped dynamic characteristics of composite structures with thicker sections and/or laminate configurations that induce interlaminar shear. The results also illustrate and quantify the significance of interlaminar shear damping in such composite structures.

Nomenclature

$[A]$, $[B^j]$, $[D^{jm}]$	= extensional, coupling, and flexural/shear laminate stiffness matrices
$[A_d]$, $[B_d^j]$, $[D_d^{jm}]$	= extensional, coupling, and flexural/shear laminate damping matrices
$[A_m]$, $[B_m^j]$, $[D_m^{jm}]$	= extensional, coupling, and flexural/shear laminate generalized mass matrices
$[C]$	= damping matrix, structural
E	= normal modulus
$F^j(z)$	= interpolation function
G	= shear modulus
h	= cross-sectional thickness
$[K]$	= stiffness matrix, structural
l	= beam length
$[M]$	= mass matrix, structural
N^o, N^j	= midplane and generalized stress resultants
$[Q]$	= composite stiffness matrix
$[R]$	= strain shape function
S	= maximum stored strain energy, per cycle
u, v, w	= axial, transverse, and through-the-thickness displacements, respectively
x, y, z	= axial, transverse, and through-the-thickness structural axes
α, β	= plate dimensions along x and y axes, respectively
ΔS	= dissipated strain energy, per cycle
$\{\epsilon\}$	= engineering strain tensor
η	= loss factor
ν	= Poisson's ratio
ρ	= mass density
ϕ	= shape function
ψ	= specific damping capacity
ω	= natural frequency

Subscripts

c	= composite (structural coordinates)
e	= element
L	= laminate
l	= composite (material coordinates)
m	= mode order, x direction
n	= mode order, y direction
1	= normal longitudinal (direction 11)
2	= normal transverse, in plane (direction 22)
3	= normal transverse, out of plane (direction 33)
4	= interlaminar shear (direction 23)
5	= interlaminar shear (direction 13)
6	= in-plane shear (direction 12)

Superscripts

j	= generalized
o	= midplane

Introduction

THE significance of passive damping in improving the dynamic performance of flexible structures requiring tight vibration control, high fatigue endurance, and accurate positioning devices and sensors has been recently emphasized. In addition, low levels of damping are also considered beneficial in actively controlled structures because they typically improve the robustness of the controller. As a result, the prediction and tailoring of the passive damping capacity of polymer matrix composite structures are receiving current attention.

Various damping mechanics theories for unidirectional composites, laminates, and structures have been reported, and a representative selection is mentioned here.[1-11] However, most of the previously mentioned work is limited to the classical laminate theory assumptions that neglect interlaminar shear effects; hence, this work is suitable only for thin laminates. Moreover, interlaminar shear effects are more critical in laminated composite structures because of their through-the-thickness inhomogeneity and anisotropy than in homogeneous isotropic materials. Therefore, interlaminar shear damping is expected to be significant in composites, particularly in laminates of thicker sections. Yet limited research has been reported in this direction.[12]

This paper presents recent developments on discrete damping mechanics enabling more accurate prediction of damping properties in thick composite structures. The modeling of damping at the laminate level is based on a novel discrete-layer laminate damping theory (DLDT) that assumes a discrete yet piecewise continuous displacement field through the laminate. The DLDT effectively captures both interply and intraply stresses. The overall damping capacity of the laminate includes contributions from extension, flexure shear, and various material coupling from possible asymmetries that may exist due to the heterogeneous nature of the composite laminate.

Semianalytical methods were first developed for the prediction of modal damping and other dynamic characteristics of thick specialty composite plates.[13] This method was exact and

Received May 11, 1992; revision received Sept. 17, 1992; accepted for publication Sept. 24, 1992.

*Senior Research Associate; mailing address: NASA Lewis Research Center, 21000 Brookpark Road, MS 49-8, Cleveland, OH 44135. Member AIAA.

computationally inexpensive, but its applications were limited. To simulate damping in composite structures of general thickness, shape, lamination, and boundary conditions, generalized structural mechanics based on finite element discretization were developed. This approach is described in the following sections. A specialty four-node element incorporating the aforementioned discrete-layer laminate damping theory is described. Generalized damping, stiffness, and mass element matrices are formulated. Therefore, in addition to improved modal damping predictions, more accurate calculations of the dynamic response and stresses may also be obtained.

Evaluations of the damping mechanics are presented. The validations include either direct comparisons with known exact solutions for composite plates or comparisons between the DLDT and classical damping theory. The significance of interlaminar shear damping contributions is also quantified. Finally, the effects of thickness and lamination on the damped dynamic characteristics of composite plates and beams are investigated.

Composite Mechanics

This section briefly reviews the synthesis of damping for on-axis composites (damping along the material axes), off-axis composites (unidirectional composites loaded at an angle), and composite laminates of general stacking sequence. The measures of damping used in this paper will be primarily the loss factor η and secondarily the specific damping capacity (SDC) ψ ($\eta = \psi/2\pi$).

Unidirectional Composites

For a unidirectional composite loaded along the material axes (see Fig. 1a), closed-form expressions have been developed for the synthesis of elastic and dissipative properties.[7] In summary, five independent elastic parameters completely characterize the stiffness of a unidirectional composite (orthotropic but transversely isotropic material). An additional four independent damping loss factors characterize the composite damping, that is, longitudinal damping η_{l11} (direction 11), transverse in-plane damping η_{l22} (direction 22), transverse through-the-thickness damping $\eta_{l33} = \eta_{l22}$ (direction 33), in-plane shear damping η_{l66} (direction 12), interlaminar shear damping η_{l44} (direction 23), and interlaminar shear damping $\eta_{l55} = \eta_{l66}$ (direction 13). Both damping and elastic properties are explicitly related to the fiber and matrix properties and to the fiber volume ratio (FVR).

For the case of off-axis composites, i.e., composites loaded at an angle θ, a 6×6 damping matrix $[\eta_c]$ best describes the damping of the composite. More details about this off-axis damping matrix are provided in the Appendix and Refs. 7 and 13. Off-axis loading affects the overall damping capacity of the composite in two distinct ways that are uncommon to isotropic materials: by altering the dissipative capability of the ply directly associated to normal and shear strains and by inducing damping coupling between normal and shear strains.

Thick Laminates

To model the damping of thick composite laminates, a discrete-layer laminate damping theory incorporating a piecewise continuous displacement field through the thickness is developed. The kinematic assumptions for the laminate theory are schematically shown in Fig. 1b. Discrete-layer or generalized laminate theories have been proposed[14,15] for the more accurate calculation of stresses in thick laminates. However, with additional developments presented herein, the DLDT combines the potential for accurate damping predictions in composite laminates while maintaining generality and elegance. The assumed displacement field has the form,

$$u(x, y, z, t) = u^o(x, y, t) + \bar{u}(x, y, z, t)$$
$$v(x, y, z, t) = v^o(x, y, t) + \bar{v}(x, y, z, t) \qquad (1)$$
$$w(x, y, z, t) = w^o(x, y, t)$$

where superscript o represents the uniform through-the-thickness midplane displacement, and the overbar indicates the through-the-thickness variation in the displacement field. Assuming that the displacements are separable functions of z, Eqs. (1) take the following form[15]:

$$u(x, y, z, t) = u^o(x, y, t) + \sum_{j=1}^{N} u^j(x, y, t)F^j(z)$$
$$v(x, y, z, t) = v^o(x, y, t) + \sum_{j=1}^{N} v^j(x, y, t)F^j(z) \qquad (2)$$
$$w(x, y, z, t) = w^o(x, y, t)$$

where u^j and v^j are displacements along the x and y directions, respectively, at the interfaces between composite plies or sublaminates (group of plies). The various $F^j(z)$ are interpolation functions. In this manner, the assumed in-plane displacement field is general, in that it may represent extensional, flexural, shear, and coupled deformations as well as interlaminar shear strains through the thickness of the laminate.

The engineering strains $\{\epsilon_c\}$ in each composite ply are directly derived from Eqs. (2):

$$\epsilon_{ci} = \epsilon^o_{ci} + \sum_{j=1}^{N} \epsilon^j_{ci}F^j(z) \qquad i = 1, 2, 6$$
$$\epsilon_{ci} = \epsilon^o_{ci} + \sum_{j=1}^{N} \epsilon^j_{ci}F^j_{,z}(z) \qquad i = 4, 5 \qquad (3)$$
$$\epsilon_{c3} = 0$$

The normal strain ϵ_{c3} is zero as a result of the assumed constant through-the-thickness deflection w. The midplane strains are given by

$$\epsilon^o_{c1} = u^o_{,x} \qquad \epsilon^o_{c2} = v^o_{,y} \qquad \epsilon^o_{c6} = u^o_{,y} + v^o_{,x}$$
$$\epsilon^o_{c4} = w^o_{,y} \qquad \epsilon^o_{c5} = w^o_{,x} \qquad (4)$$

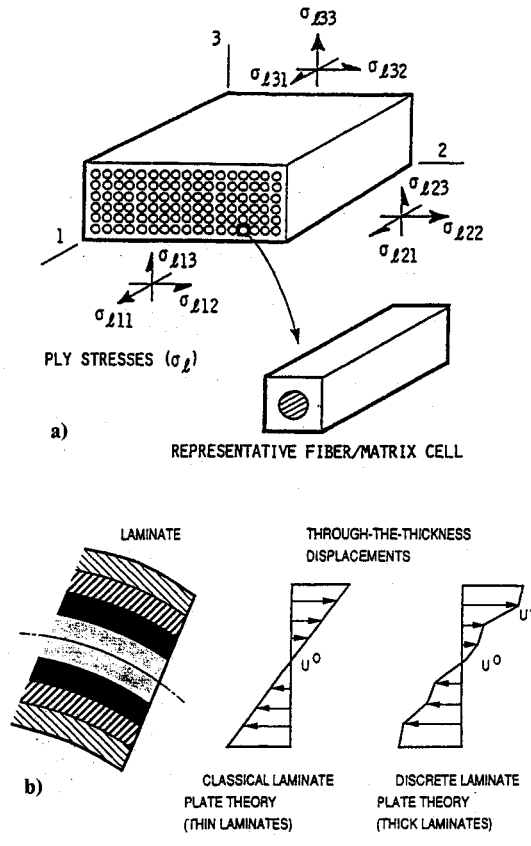

Fig. 1 a) Unidirectional composite and b) kinematic assumptions of laminate damping theories, classical laminate damping theory, and discrete-layer damping theory.

and the generalized strains are

$$\epsilon^j_{c1} = u^j_{,x} \qquad \epsilon^j_{c2} = v^j_{,y} \qquad \epsilon^j_{c6} = u^j_{,y} + v^j_{,x}$$
$$\epsilon^j_{c4} = v^j \qquad \epsilon^j_{c5} = u^j \tag{5}$$

The comma in the subscripts indicates differentiation.

The dissipated strain energy per unit area of the laminate ΔS_L is

$$\Delta S_L = \frac{1}{2}\int_{-h/2}^{h/2} 2\pi \epsilon_c^T [Q_c][\eta_c]\epsilon_c \, dz \tag{6}$$

where $[Q_c]$ is the off-axis composite stiffness matrix. Combination of Eqs. (6) and (2-5) ultimately provides the dissipated strain energy per unit area,

$$\Delta S_L = \tfrac{1}{2}2\pi\left(\epsilon_c^{oT}[A_d]\epsilon_c^o + 2\epsilon_c^{oT}\sum_{j=1}^{N}[B_d^j]\epsilon_c^j + \sum_{j=1}^{N}\sum_{m=1}^{N}\epsilon_c^{jT}[D_d^{jm}]\epsilon_c^m\right) \tag{7}$$

where $[A_d]$ includes out-of-plane shear terms. The generalized coupling damping matrices $[B_d^j]$ and flexural/shear matrices $[D_d^{jm}]$ are new. The matrix expressions in Eq. (7) are given by

$$[A_d] = \sum_{k=1}^{N_l}\int_{h_{k-1}}^{h_k}[Q_c]_k[\eta_c]_k \, dz$$
$$[B_d^j]_{in} = \sum_{k=1}^{N_l}\int_{h_{k-1}}^{h_k}([Q_c]_k[\eta_c]_k)_{in}F^j(z)\, dz \qquad i,n = 1, 2, 6$$
$$[B_d^j]_{in} = \sum_{k=1}^{N_l}\int_{h_{k-1}}^{h_k}([Q_c]_k[\eta_c]_k)_{in}F^j_{,z}(z)\, dz \qquad i,n = 4, 5 \tag{8}$$
$$[D_d^{jm}]_{in} = \sum_{k=1}^{N_l}\int_{h_{k-1}}^{h_k}([Q_c]_k[\eta_c]_k)_{in}F^j(z)F^m(z)\, dz \qquad i,n = 1, 2, 6$$
$$[D_d^{jm}]_{in} = \sum_{k=1}^{N_l}\int_{h_{k-1}}^{h_k}([Q_c]_k[\eta_c]_k)_{in}F^j_{,z}(z)F^m_{,z}(z)\, dz \qquad i,n = 4, 5$$

Similarly, the maximum laminate strain energy per unit area S_L is by definition

$$S_L = \frac{1}{2}\int_{-h/2}^{h/2}\epsilon_c^T[Q_c]\epsilon_c \, dz \tag{9}$$

Combination of Eqs. (3-5) and (9) provides the maximum strain energy as a separable form of material properties and strains,

$$S_L = \tfrac{1}{2}\left(\epsilon_c^{oT}[A]\epsilon_c^o + 2\epsilon_c^{oT}\sum_{j=1}^{N}[B^j]\epsilon_c^j + \sum_{j=1}^{N}\sum_{m=1}^{N}\epsilon_c^{jT}[D^{jm}]\epsilon_c^m\right) \tag{10}$$

where $[A]$ has additional out-of-plane shear terms.[15] The matrix expressions are given by

$$[A] = \sum_{k=1}^{N_l}\int_{h_{k-1}}^{h_k}[Q_c]_k \, dz$$
$$[B^j]_{in} = \sum_{k=1}^{N_l}\int_{h_{k-1}}^{h_k}([Q_c]_k)_{in}F^j(z)\, dz \qquad i,n = 1, 2, 6$$
$$[B^j]_{in} = \sum_{k=1}^{N_l}\int_{h_{k-1}}^{h_k}([Q_c]_k)_{in}F^j_{,z}(z)\, dz \qquad i,n = 4, 5 \tag{11}$$
$$[D^{jm}]_{in} = \sum_{k=1}^{N_l}\int_{h_{k-1}}^{h_k}([Q_c]_k)_{in}F^j(z)F^m(z)\, dz \qquad i,n = 1, 2, 6$$
$$[D^{jm}]_{in} = \sum_{k=1}^{N_l}\int_{h_{k-1}}^{h_k}([Q_c]_k)_{in}F^j_{,z}(z)F^m_{,z}(z)\, dz \qquad i,n = 4, 5$$

Considering Eq. (2), the laminate kinetic energy per unit area takes the form

$$K_L = \tfrac{1}{2}\left(\{\dot{u}^o\}^T[A_M]\{\dot{u}^o\} + 2\{\dot{u}^o\}^T\sum_{j=1}^{N}[B_M^j]\{\dot{u}^j\} + \sum_{j=1}^{N}\sum_{m=1}^{N}\{\dot{u}^j\}^T[D_M^{jm}]\{\dot{u}^m\}\right) \tag{12}$$

where the generalized laminate mass and inertia matrices are defined as

$$[A_M] = \sum_{k=1}^{N_l}\int_{h_{k-1}}^{h_k}\mathrm{diag}(\rho_k)\, dz$$
$$[B_M^j] = \sum_{k=1}^{N_l}\int_{h_{k-1}}^{h_k}\mathrm{diag}(\rho_k)F^j(z)\, dz \tag{13}$$
$$[D_M^{jm}] = \sum_{k=1}^{N_l}\int_{h_{k-1}}^{h_k}\mathrm{diag}(\rho_k)F^j(z)F^m(z)\, dz$$

The term $\mathrm{diag}(\rho_k)$ indicates a diagonal matrix, with all diagonal terms equal to the density of the kth ply. The kinetic energy in Eq. (12) includes contributions of rotational inertia. As seen, the proposed laminate damping mechanics are general, and they can handle any laminate configuration in terms of composite plies, ply angles, laminate stacking sequence, and thickness.

Simply Supported Composite Plates

Based on the laminate mechanics just described, exact solutions of the damped dynamic characteristics for specialty composite plates have been obtained and summarized herein for the sake of completeness.[13] These exact and computationally inexpensive predictions of static and dynamic characteristics (modal damping, natural frequencies) provide valuable insight into the mechanics of the problem and establish a baseline for validating approximate numerical methods. Most other laminations, boundary conditions, and structural configurations require approximate discretized solutions, and such finite element based computational mechanics are described in the next section.

For a rectangular $\alpha \times \beta$ simply supported (SS) composite plate with negligible coupling ($A_{16} = A_{26} = 0$, $B^j_{16} = B^j_{26} = 0$, $D^{jm}_{16} = D^{jm}_{26} = 0$), the following Navier fundamental solutions form a complete set of mode shapes in the x-y plane:

$$u^0_{mn}(x, y, t) = U^0_{mn}\cos(ax)\sin(by)e^{i\omega t}$$
$$v^0_{mn}(x, y, t) = V^0_{mn}\sin(ax)\cos(by)e^{i\omega t}$$
$$w^0_{mn}(x, y, t) = W^0_{mn}\sin(ax)\sin(by)e^{i\omega t} \tag{14}$$
$$u^j_{mn}(x, y, t) = U^j_{mn}\cos(ax)\sin(by)e^{i\omega t}$$
$$v^j_{mn}(x, y, t) = V^j_{mn}\sin(ax)\cos(by)e^{i\omega t}$$

where $a = m\pi/\alpha$, $b = n\pi/\beta$, and the fundamental solutions in Eq. (14) are chosen because they satisfy the boundary conditions of the simply supported plate.

Combination of Eqs. (4), (5), and (14) yields the modal midplane and generalized strains as separable functions of x, y coordinates, time, and amplitudes:

$$\{\epsilon^o\}_{mn} = [B^o_{mn}]\{U^o_{mn}\}e^{i\omega t} \qquad \{\epsilon^j\}_{mn} = [B^j_{mn}]\{U^j_{mn}\}e^{i\omega t} \tag{15}$$

where the terms in matrices $[B_{mn}]$ are sinusoidal functions of x, y coordinates and mode order. The amplitude displacement vectors are $\{U^o\} = \{U^o, V^o, W^o\}^T$ and $\{U^j\} = \{U^j, V^j\}^T$.

By substituting Eqs. (15) into the strain and kinetic energy expressions for the laminate, Eqs. (10) and (12), respectively, integrating over the plate area, and applying Lagrangian dynamics, the modal analysis (free vibration) solution of the plate takes the form

$$-\omega_{mn}^2[M_{mn}]U_{mn} + [K_{mn}]U_{mn} = 0 \tag{16}$$

where the through-the-thickness modal displacements are $\{U_{mn}\} = \{U_{mn}^o; U_{mn}^1, \ldots, U_{mn}^N\}$. Numerical solution of this eigenvalue problem provides the natural frequencies ω_{mn} and the through-the-thickness modes $\{U_{mn}\}$ for each order mn of plane modes, in the context of Eqs. (14).

The modal damping associated with the mnth vibration mode η_{mn} is

$$\eta_{mn} = \frac{1}{2\pi}\frac{\int_A \Delta S_{Lmn}\, dA}{\int_A S_{Lmn}\, dA} \tag{17}$$

where ΔS_{Lmn} and S_{Lmn} are the dissipated and maximum laminate strain energies of the associated mode.

Finite Element Method

Computational finite element based mechanics for the damping analysis of thick composite structures of general laminations and shapes were developed, based on the DLDT, and are summarized herein. In view of the generalized laminate strains and stresses described in the preceding sections, the variational formulation of the equilibrium equations for the candidate structure takes the form

$$\begin{aligned}
&-\int_A \left\{\delta\epsilon^{oT}N^o + \sum_{j=1}^{N}\delta\epsilon^{jT}N^j\right\} dA \\
&-\int_A \left\{\delta u^{0T}[A_m]\ddot{u}^o + 2\delta u^{0T}\sum_{i=1}^{N}[B_m^j]\ddot{u}^j \right. \\
&\left. + \sum_{j=1}^{N}\sum_{m=1}^{N}\delta u^{jT}[D_m^{jm}]\ddot{u}^m\right\} dA + \delta u_i^T F_i \\
&+\int_S \delta u_s^T F_s\, ds = 0
\end{aligned} \tag{18}$$

For viscoelastic constituents, the constitutive viscoelastic law between generalized stresses and strains at the laminate level may be eventually expressed by the following convolute products,

$$\begin{aligned}
N^o(t) &= [\tilde{A}(t)]*\epsilon^o(t) + \sum_{m=1}^{N}[\tilde{B}^m(t)]*\epsilon^m(t) \\
N^j(t) &= [\tilde{B}^j(t)]*\epsilon^o(t) + \sum_{m=1}^{N}[\tilde{D}^{jm}(t)]*\epsilon^m(t), \qquad j = 1, \ldots, N
\end{aligned} \tag{19}$$

where $*$ indicates a convolution operation, for example,

$$\sigma_c = [\tilde{Q}_c]*\epsilon_c = \int_{-\infty}^{t}[\tilde{Q}(t-\tau)]\, d\epsilon(\tau) \tag{20}$$

Hence, the first left-hand integral in Eq. (18) represents both stored and dissipated strain energies during the virtual displacement. The elastic laminate relations will result from Eq. (19) if time effects are neglected. Also, viscous damping is a special case of Eq. (18). In the frequency domain (harmonic vibration), Eqs. (19) will result in equivalent expressions of complex laminate stiffness, with storage and loss stiffness matrices described in Eqs. (8) and (11), respectively.

The variational relationship may be discretized to an approximate equivalent system of dynamic equations, if the reference and generalized displacements are discretized as follows:

$$\begin{aligned}
\{u^o, v^o, w^o\} &= \sum_{i=1}^{\text{nodes}}[\Phi_i]\{u_i^o, v_i^o, w_i^o\} \\
\{u^j, v^j\} &= \sum_{i=1}^{\text{nodes}}[\Phi_i]\{u_i^j, v_i^j\}, \qquad j = 1, \ldots, N
\end{aligned} \tag{21}$$

where subscript i indicates the ith node, and the various Φ_i are interpolating functions. The reference and generalized strain shape functions, $[R^o]_i$ and $[R]_i$ interpolating the strains to the nodal displacements, are obtained by differentiating Eq. (21) in accordance with Eqs. (4) and (5). Then the damping or loss element matrix $[C_{eij}]$ for nodes i and j takes the following form:

$$[C_{eij}] = \int_{A_e}\begin{bmatrix} R_i^{oT}[A_d]R_j^o & R_i^{oT}[B_d^1]R_j & \cdots & R_i^{oT}[B_d^N]R_j \\ R_i^T[B_d^1]R_j^o & R_i^T[D_d^{ij}]R_j & \cdots & R_i^T[D_d^{1N}]R_j \\ \cdot & \cdot & \cdots & \cdot \\ \cdot & \cdot & \cdots & \cdot \\ R_i^T[B_d^N]R_i^o & R_i^T[D_d^{Nl}]R_j^o & \cdots & R_i^T[D_d^{NN}]R_j \end{bmatrix} dA_e \tag{22}$$

where A_e is the area of the element. The area integration is performed numerically. The stiffness and mass matrices of the element, $[K_{eij}]$ and $[M_{eij}]$, respectively, have analogous forms. Subsequently, the dissipated and maximum stored strain energies of the element are given by

$$\Delta S_{eij} = \tfrac{1}{2}U_i^T[C_{eij}]U_j, \qquad S_{eij} = \tfrac{1}{2}U_i^T[K_{eij}]U_j \tag{23}$$

and the modal damping of the nth mode η_n is expressed as the ratio of the dissipated over the maximum modal strain energy of the structure:

$$\eta_n = \frac{1}{2\pi}\frac{\Sigma\Delta S_{eijn}}{\Sigma S_{eijn}} \tag{24}$$

In this context, a bilinear four-node plate element was developed. Selective integration was used to avoid overstiffening of the element in the case of low thickness. Such overstiffening was observed with full integration.

Applications and Discussion

To demonstrate the quality and versatility of the composite mechanics, applications on graphite/epoxy composite plates and beams were performed. When applicable, numerical results obtained with the aforementioned element were compared with the exact solutions. In all other cases, the predictions were compared with results obtained using a triangular plate element based on classical laminate damping theory (CLDT).[11] Both elements will be referred to, respectively, as DLDT and CLDT finite elements hereafter. The composite material used in all applications was HM-S graphite/epoxy of 50% FVR, with typical mechanical properties shown in Table 1. Measured data for this composite are provided in Ref. 9. The properties of the fibers and the matrix were backcalculated using micromechanics[9] to match the measured properties of the composite. Unless otherwise stated, the nominal thickness of each composite ply was taken as 0.254 mm (0.01 in.).

$[0_4/90_4]_s$ Simply Supported Composite Plate

Figure 2 shows predicted natural frequencies and modal damping values of the fundamental mode of a $[0_4/90_4]_s$ square composite simply supported (SS) plate as functions of thickness aspect ratio (a/h), where h is the plate thickness. The modal characteristics of the first four modes, that is, modes

Table 1 Mechanical properties of the HM-S/epoxy system

Epoxy	HM-S graphite	HM-S/epoxy[9] (0.50 FVR), %
E = 0.500 Mpsi (3.45 GPa)	E_{f11} = 55.0 Mpsi (379.3 GPa)	η_{l11} = 0.072
G = 0.185 Mpsi (1.27 GPa)	E_{f22} = 0.9 Mpsi (6.2 GPa)	η_{l22} = 0.670
	G_{f66} = 1.1 Mpsi (7.6 GPa)	η_{l44} = 1.120
	ν_{f12} = 0.20	η_{l66} = 1.120

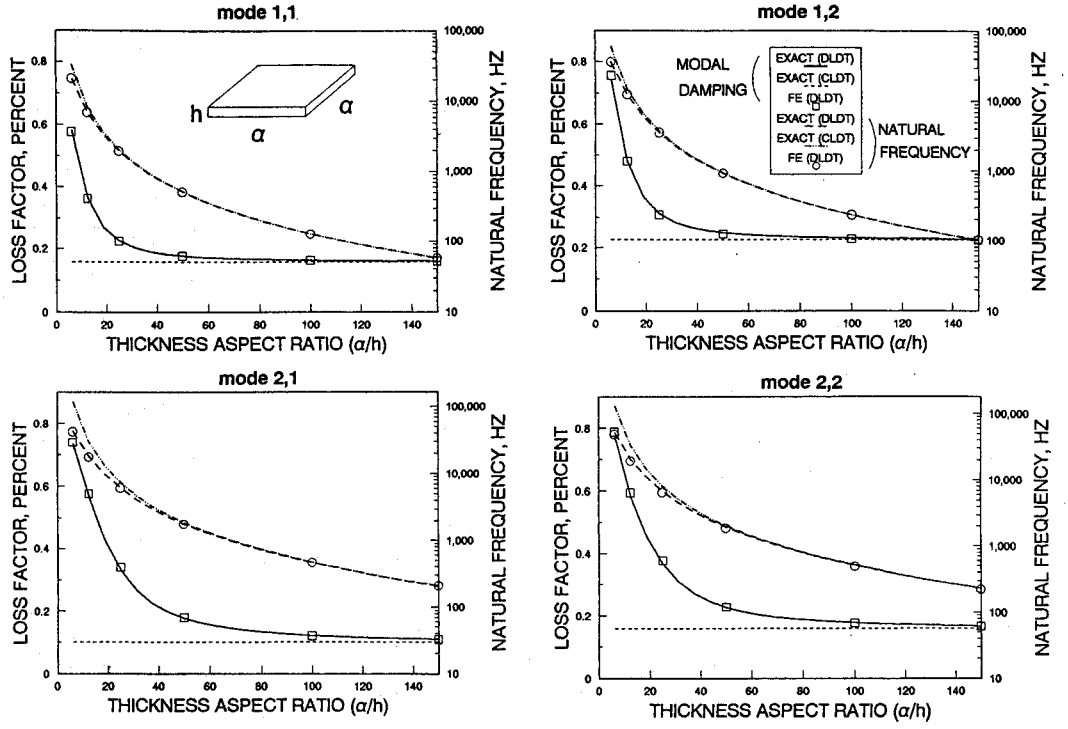

Fig. 2 Modal characteristics of a $[0_4/90_4]_s$ graphite/epoxy simply supported plate.

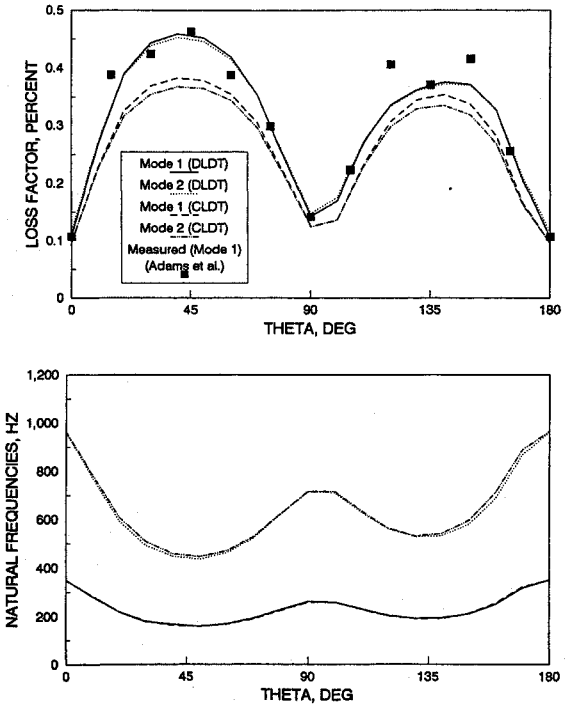

Fig. 3 Modal characteristics of a $[\theta/90 + \theta/45 + \theta/-45 + \theta]_s$ cantilever beam ($l/h = 125$; $l = 8$ in.); first and second bending modes.

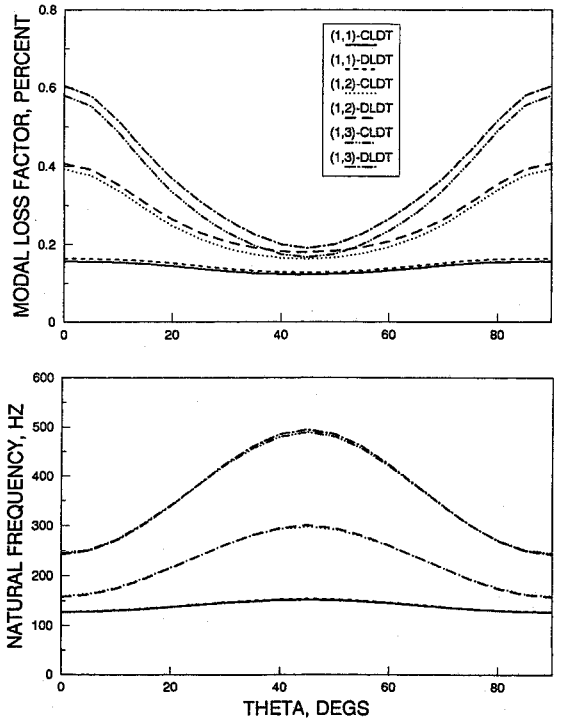

Fig. 4 Modal characteristics of a $[\theta_4/-\theta_4]_s$ graphite/epoxy simply supported plate ($\alpha/h = 100$).

(1, 1), (1, 2), (2, 1), and (2, 2), are shown, respectively. It is pointed out that this laminate has different flexural damping and stiffness characteristics in x and y directions; thus modes (1, 2) and (2, 1) have different natural frequencies and modal loss factors. The finite element model consisted of a uniform mesh of 8×8 element subdivisions. Clearly, there is excellent agreement between the exact DLDT solutions and the finite element model in the shown thickness regime. The exact CLDT solution is also shown to illustrate the significant differences between the two theories in damping prediction at high thicknesses. The differences between DLDT and CLDT predictions provide the estimate of interlaminar shear damping. Finally, the results calculated using the DLDT finite element converge to the exact CLDT predictions as the plate thickness is decreased.

$[0/90/45/-45]_s$ Free-Free Composite Beam

Figure 3 presents the modal damping and natural frequencies of the first and second bending modes of an unsupported (free-free) $[\theta/90 + \theta/45 + \theta/-45 + \theta]_s$ thin beam ($l/h = 125$). This laminate configuration was used previously in both experimental and analytical studies.[8,9] The CLDT model has failed to capture the portion of damping due to interlaminar shear stresses and relative rotation between adjacent plies.

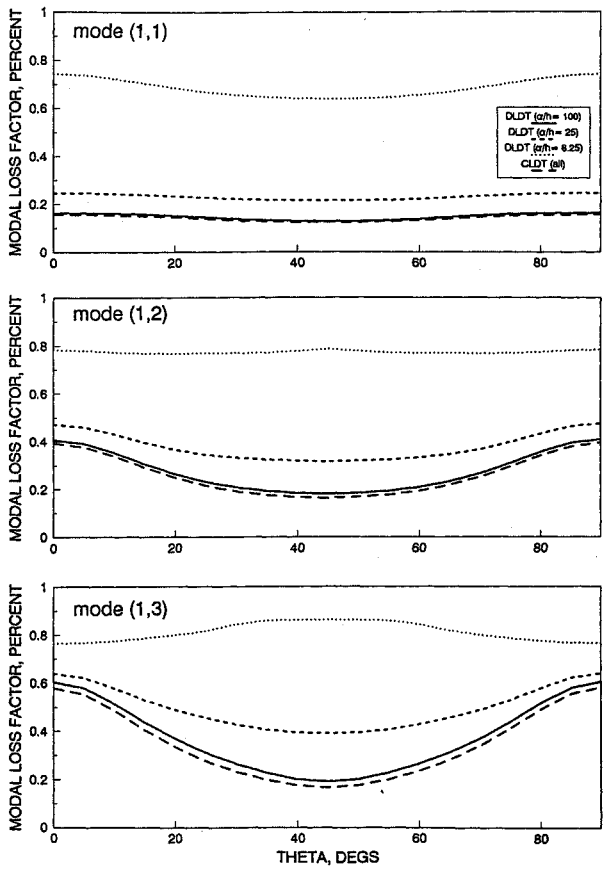

Fig. 5 Effect of thickness aspect ratio on the modal damping of a $[\theta_4/-\theta_4]_s$ graphite/epoxy simply supported plate.

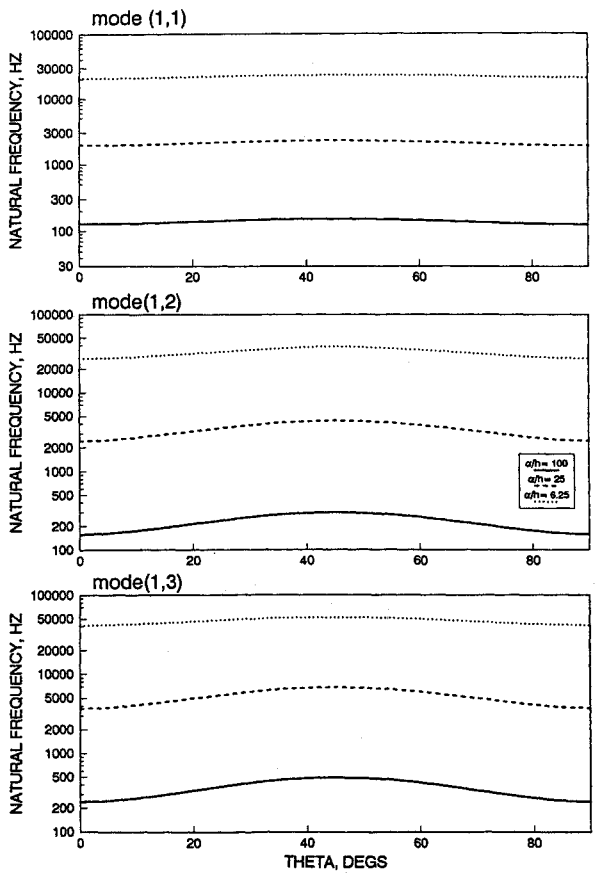

Fig. 6 Effect of thickness aspect ratio on the natural frequencies of a $[\theta_4/-\theta_4]_s$ graphite/epoxy simply supported plate.

Hence, this case serves as a demonstration of the dependence of damping on the specific laminate lay-up only and also as an example of the capacity of DLDT to capture both flexural and shear damping.

Equivalent element meshes consisting of 15×4 element subdivisions were used to predict the dynamic characteristics of the beam. The dimensions of the beam were approximately equal to specimens used by Ni and Adams,[9] that is, 200 mm (8 in.) long, 12 mm (0.5 in.) wide, and 1.60 mm (0.064 in.) thick. As seen in Fig. 3, the DLDT damping predictions are higher than the CLDT prediction and correlate very well with the reported measurements[9]; hence, the new theory has succeeded in capturing the interlaminar shear damping contributions in the range of high interlaminar shear stresses and relative rotation between outer plies ($\theta \simeq 45$ and 135 deg). It is emphasized that in this case the interlaminar shear damping is mostly the result of inhomogeneities in the material anisotropy between the plies of alternating fiber orientation; therefore, the case study serves as another example of the superiority of the method.

$[\theta_4/-\theta_4]_s$ Simply Supported Composite Plate

The lower modal damping values and natural frequencies predicted for a simply supported $[\theta_4/-\theta_4]_s$ graphite/epoxy plate are shown in Fig. 4. A uniform 8×8 finite element mesh was again used to model the plate. The modes are identified with their shape at $\theta = 0$. The plate is rather thin ($\alpha/h = 100$); therefore, the predictions with both DLDT and CLDT finite elements were expected to be similar. Yet the DLDT element resulted in higher predictions of damping with respect to the CLDT element as a result of the additional shear contributions. The difference in damping predictions, which indicates the contributions of shear damping, increased with the order of the mode. It seems that the interlaminar shear damping contributions are slightly higher for fiber orientations around $\pm$ 45 deg, which corresponds to lay-ups with higher interlaminar shear stresses, indicating the advantage of DLDT in representing interlaminar shear damping.

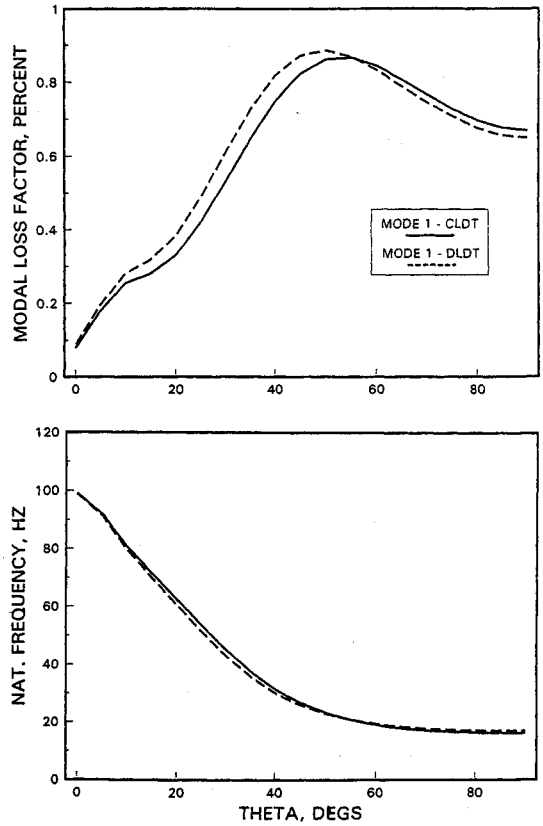

Fig. 7 Fundamental modal characteristics of a $[\theta_5/-\theta_5]_s$ graphite/epoxy cantilever beam ($l/h = 60$).

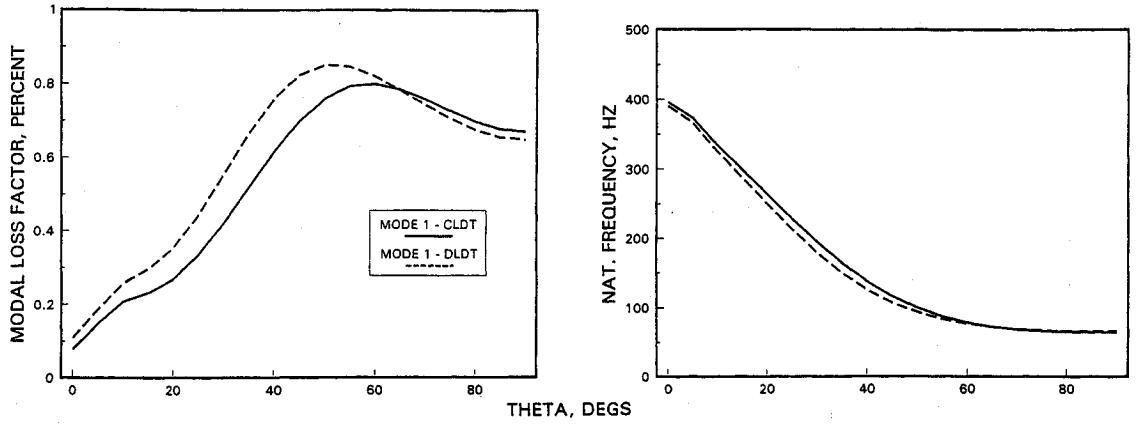

Fig. 8 Fundamental modal characteristics of a $[\theta_5/-\theta_5]_s$ graphite/epoxy cantilever beam ($l/h = 30$).

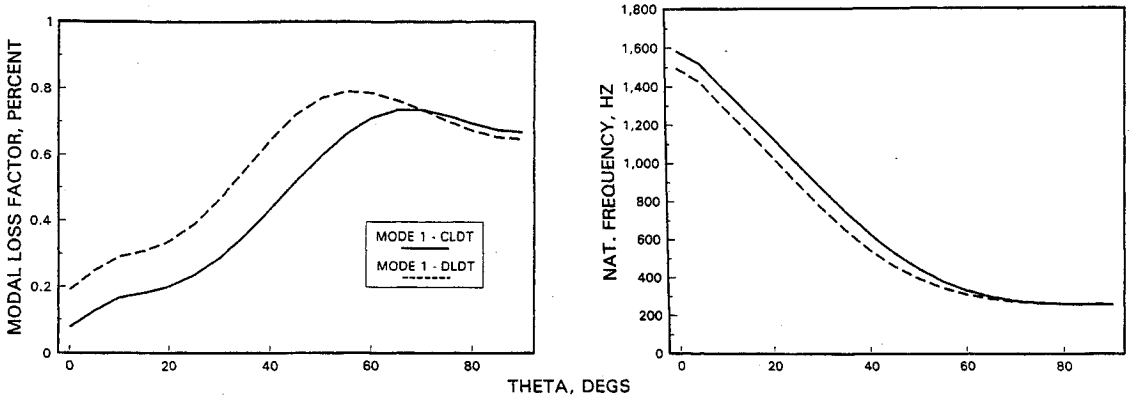

Fig. 9 Fundamental modal characteristics of a $[\theta_5/-\theta_5]_s$ graphite/epoxy cantilever beam ($l/h = 15$).

To investigate further the dependence of interlaminar shear damping on the laminate lay up, the modal damping of the preceding three modes is shown in Fig. 5 for plates of various thickness. The damping predictions of the CLDT model, which are independent of thickness, are also plotted. The corresponding natural frequencies are shown in Fig. 6. Keeping in mind that the differences between DLDT and CLDT results indicate the magnitude of shear damping, there is definite coupling between laminate lay-up and thickness, especially in the second and third mode. The interlaminar shear damping is again higher at ± 45 deg where the interlaminar stresses are highest. In this manner, the results provide additional confidence and value to the damping mechanics.

$[\theta_5/-\theta_5]_s$ Cantilever Composite Beams

Figures 7–9 present the predicted fundamental modal damping and natural frequency of $[\theta_5/-\theta_5]_s$ cantilever beams with thickness aspect ratios l/h of 60, 30, and 15, respectively. The width and thickness of the beams were 25.4 mm (1 in.) and 0.508 mm (0.2 in.), respectively. The same uniform mesh consisting of 15×4 element subdivisions was used in all cases. For ply angles between 0 and 60 deg, the DLDT model yielded significantly higher predictions of damping and lower predictions of natural frequency in the cases of thicker beams ($l/h = 15$). These differences were attributed to the high interlaminar stresses at the higher thickness beams. The coupling between lay-up and thickness of the beam is also illustrated in Fig. 9. The results demonstrate again the quality of the method in predicting shear effects due to thickness, laminate lay-up, or combinations of both.

Summary

Computational mechanics for the analysis of damping and other dynamic characteristics of thick composite structures were developed and described. The damping mechanics included micromechanics, discrete laminate mechanics, and finite element based structural mechanics for composite structures of thicker cross sections and/or structures with laminate configurations with significant interlaminar shear stresses. A specialty four-node bilinear element with damping analysis capabilities was developed and embedded into an in-house research code.

Applications on composite plates and beams demonstrated the quality of the methodology and its effectiveness in simulating the damping of composite structures of high thickness. The potential of the method in capturing the effects of interlaminar shear damping due to higher interlaminar stresses as the result of the laminate configuration was also illustrated. Apart from the effectiveness of the mechanics, the case studies revealed the strong sensitivity of structural composite damping to thickness, laminate configuration, and mode order and, furthermore, the strong interrelationship between them. As a result of this interrelationship, it seems premature to set quantitative guidelines regarding the limitations of the classical damping theory, and the readers are encouraged to apply their engineering judgment based on the reported results. In addition, damping was proved to be far more sensitive to interlaminar shear phenomena than natural frequencies. The developed integrated structural mechanics appear to be very promising for the analysis of passive damping in thick composite structures. Additional studies regarding the significance of interlaminar shear damping on typical propulsion composite structures are planned for the near future.

Appendix

The off-axis ply stiffness matrix $[Q_c]$ is

$$\{\sigma_c\} = [Q_c]\{e_c\} \tag{A1}$$

$$[Q_c] = [R]^{-1}[Q_l][R]^{-T} \tag{A2}$$

where $[Q_l]$ is the stiffness matrix in the material axes. The transformation matrices are

$$[R] = \begin{bmatrix} m^2 & n^2 & 0 & 0 & 0 & 2mn \\ n^2 & m^2 & 0 & 0 & 0 & -2mn \\ 0 & 0 & 1 & 0 & 0 & 0 \\ 0 & 0 & 0 & m & -n & 0 \\ 0 & 0 & 0 & n & m & 0 \\ -mn & mn & 0 & 0 & 0 & m^2 - n^2 \end{bmatrix}$$

$$m = \cos\theta, \qquad n = \sin\theta \tag{A3}$$

$$[R]^{-1} = [R(-\theta)] \tag{A4}$$

The on-axis damping matrix is

$$[\eta_l] = \text{diag}[\eta_{l11}, \eta_{l22}, \eta_{l33}, \eta_{l44}, \eta_{l55}, \eta_{l66}] \tag{A5}$$

The off-axis ply damping matrix is

$$[\eta_c] = [R]^T[\eta_l][R]^{-T} \tag{A6}$$

$$[\eta_c] = \begin{bmatrix} \eta_{c11} & \eta_{c12} & 0 & 0 & 0 & \eta_{c16} \\ \eta_{c21} & \eta_{c22} & 0 & 0 & 0 & \eta_{c26} \\ 0 & 0 & \eta_{c33} & 0 & 0 & 0 \\ 0 & 0 & 0 & \eta_{c44} & \eta_{c45} & 0 \\ 0 & 0 & 0 & \eta_{c54} & \eta_{c55} & 0 \\ \eta_{c61} & \eta_{c62} & 0 & 0 & 0 & \eta_{c66} \end{bmatrix} \tag{A7}$$

Acknowledgments

This work was supported by NASA Grant NCC3-208/4. This support is gratefully acknowledged. The author also wants to acknowledge the contributions of Christos C. Chamis, senior aerospace scientist at NASA Lewis Research Center, for his valuable comments and discussions.

References

[1]Hashin, Z., "Complex Moduli of Viscoelastic Composites—II. Fiber Reinforced Composite Materials," *International Journal of Solids and Structures,* Vol. 6, No. 6, 1970, pp. 797–807.

[2]Schultz, A. B., and Tsai, S. W., "Measurements of Complex Dynamic Moduli for Laminated Fiber-Reinforced Composites," *Journal of Composite Materials,* Vol. 3, July 1969, pp. 434–443.

[3]Adams, R. D., Fox, M. A. O., Flood, R. J. L., Friend, R. J., and Hewitt, R. L., "The Dynamic Properties of Unidirectional Carbon and Glass Fiber-Reinforced Plastics in Torsion and Flexure," *Journal of Composite Materials,* Vol. 3, Oct. 1969, pp. 594–603.

[4]Siu, C. C., and Bert, C. W., "Sinusoidal Response of Composite-Material Plates with Material Damping," *ASME Journal of Engineering for Industry,* Vol. 96, No. 2, May 1974, pp. 603–610.

[5]Sun, C. T., Chaturvedi, S. K., and Gibson, R. F., "Internal Damping of Short-Fiber Reinforced Polymer Matrix Composites," *Computers and Structures,* Vol. 20, No. 1-3, 1985, pp. 391–400.

[6]Suarez, S. A., Gibson, R. F., Sun, C. T., and Chaturvedi, S. K., "The Influence of Fiber Length and Fiber Orientation on Damping and Stiffness of Polymer Composite Materials," *Experimental Mechanics,* Vol. 26, No. 2, 1986, pp. 175–184.

[7]Saravanos, D. A., and Chamis, C. C., "Unified Micromechanics of Damping for Unidirectional and Off-Axis Fiber Composites," *Journal of Composites Technology and Research,* Vol. 12, No. 1, 1990, pp. 31–40.

[8]Saravanos, D. A., and Chamis, C. C., "Mechanics of Damping for Fiber Composite Laminates Including Hygro-Thermal Effects," *AIAA Journal,* Vol. 28, No. 10, 1990, pp. 1813–1819.

[9]Ni, R. G., and Adams, R. D., "The Damping and Dynamic Moduli of Symmetric Laminated Composite Beams—Theoretical and Experimental Results," *Journal of Composite Materials,* Vol. 18, No. 2, 1984, pp. 104–121.

[10]Bicos, A. S., and Springer, G. S., "Vibrational Characteristics of Composite Panels with Cutouts," *AIAA Journal,* Vol. 27, No. 8, 1989, pp. 1116–1122.

[11]Saravanos, D. A., and Chamis, C. C., "Computational Simulation of Damping in Composite Structures," *Journal of Reinforced Plastics and Composites,* Vol. 10, No. 3, 1991, pp. 256–278.

[12]Alam, N., and Asnani, N. T., "Vibration and Damping Analysis of Fibre Reinforced Composite Material Plates," *Journal of Composite Materials,* Vol. 20, No. 1, 1986, pp. 2–18.

[13]Saravanos, D. A., and Pereira, J. M., "The Effects of Interlaminar Damping Layers on the Dynamic Response of Composite Structures," *AIAA Journal,* Vol. 30, No. 12, 1992, pp. 2906–2913.

[14]Noor, A. K., and Burton, S. W., "Assessment of Computational Models for Multilayer Composite Shells," *Applied Mechanics Reviews,* Vol. 43, No. 4, 1990, pp. 67–96.

[15]Barbero, E. J., Reddy, J. N., and Teply, J., "An Accurate Determination of Stresses in Thick Composite Laminates Using a Generalized Plate Theory," *International Journal for Numerical Methods in Engineering,* Vol. 29, Jan. 1990, pp. 1–14.